

Duong Van NGUYEN ^{1,2}, Chien Quoc NGUYEN ¹,
Hieu Van DANG ², Hoang Manh CHU ¹

Design and performance analysis of a mechanically coupled spring compliant to out-of-plane oscillation

Received 11 February 2022, Revised 30 May 2022, Accepted 7 June 2022, Published online 16 November 2022

Keywords: coupled spring, mode coupling, serpentine spring, Sigitta spring theory, finite element method

In this paper, a spring system symmetrically arranged around a circular plate compliant to out-of-plane oscillation is proposed. The spring system consists of single serpentine springs mutually coupled in a plane. Three theoretical mechanical models for evaluating the stiffness of the spring system are built, which are based on the flexural beam, Sigitta, and serpentine spring theories and equivalent mechanical spring structure models. The theoretically calculated results are in good agreement with numerical solutions using the finite element method, with errors less than 10% in the appropriate dimension ranges of the spring. Compared to similar spring structures without mechanical coupling, the proposed mechanically coupled spring shows advantage in suppressing the mode coupling.

1. Introduction

The mechanical spring is a key element in various micro-electro-mechanical systems (MEMS) devices such as micro-actuators, inertial switches, accelerometers, and so on [1–17]. In these devices, mechanical springs are designed for single or multi-axis motion. Up to date, there are many types of springs introduced for applications in controlling in-plane motions [1–17]. The springs can be designed for compliance to the linear movements in x and y axes [1–4, 7, 9, 12]. In these

✉ Hoang Manh Chu, e-mails: hoang.chumanh@hust.edu.vn, hoangcm@itims.edu.vn

¹International Training Institute for Materials Science, Hanoi University of Science and Technology, Vietnam. ORCID: D.V.N.: 0000-0003-3880-9828; C.Q.N.: 0000-0001-8521-1146; H.M.C.: 0000-0001-5808-8736

²FPT University, Hanoi, Vietnam, H.V.D. ORCID: 0000-0001-7774-775X



designs, the springs are normally composed of the straight beams [1] and a few designs employed the serpentine beam for extending the movement in the x and y axes [10]. For the rotational motion, the straight beam and serpentine springs have also been used [18–22]. In general, the component spring elements are independent to each other, one end of component spring element connected to a proof-mass/structure while the other is fixed to substrate or connected to another structure. For out-of-plane z -axis motion, the straight beam springs have been employed, however, their displacement range is limited [1, 23, 24]. To extend the out-of-plane movement range in micro-actuators while minimizing the device area, serpentine beam and spiral springs have been introduced [12–14]. In the design of micro-actuators, the stiffness of suspending springs needs to be determined for evaluating the operational frequency range as well as their actuation voltage [1–4, 11–13, 18]. In the mechanical sensors, the sensitivity is defined by the stiffness of suspending springs [14]. The different devices require the different operational frequency range. The inertial switches need fast response time on order of μs , i.e., the operational frequency at hundreds of kHz [3, 15]. In the MEMS accelerometers, the operational frequency range is from 0.1 Hz to 10^4 Hz, for applications from inertial navigation to explosion monitoring [16]. To evaluate the stiffness of suspending springs, theories of elastic straight beam, the Sigitta spring, and serpentine spring have been applied [1, 14, 25, 26]. In particular, recently an actuator for out-of-plane displacement has been proposed and investigated by the finite element method (FEM). The spring with straight beams arranged around a square plate and coupled with each other has shown that the operational frequency range can be extended while the coupling between the operation and undesired oscillation modes is suppressed [11]. However, the coupled curve springs and theoretical models for evaluating the stiffness of this spring system have not yet been much studied for low mode cross-talk micro-actuators and low-noise mechanical sensors.

In this paper, we present a novel design of a spring system arranged around a circular plate compliant to out-of-plane z -axis oscillation. We use single serpentine beam springs and couple them with each other to suppress undesired oscillation modes while the design guarantees compliance to the z -axis oscillation. The performance of the spring is investigated by FEM and compared to the other similar spring structures without mechanical coupling. The theoretical mechanical models for evaluating the stiffness of the spring system are built, and the calculated results are compared to numerical solutions using FEM.

2. Spring model compliant to out-of-plane z -axis oscillation

The coupled spring is composed of six serpentine springs that are symmetrically arranged around a center plate forming a circular spring system, Fig. 1. The serpentine springs are linked together at meandering beams/circular arcs. For convenience in presentation, this coupled spring is called to be Type A. The parameters of Type A are also shown in Figs 1a and 1b, where w and t are the width

and thickness of the spring circular arcs, L_{IS} is the length of beam interconnecting between the serpentine spring arcs, L_{IB} is the length of beam interconnecting between spring circular arcs in each serpentine spring, which is also the gap between spring arcs, and R ($= 50 \mu\text{m}$) is the radius of the center plate.

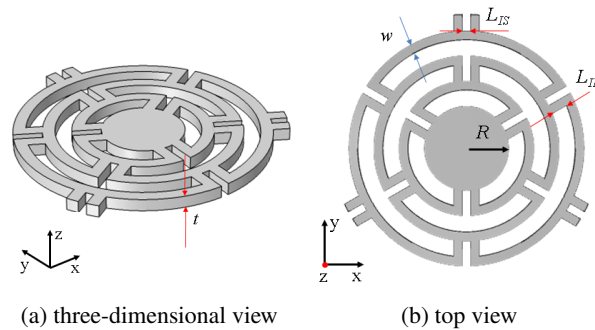


Fig. 1. Proposed coupling spring with curved beams and design parameters

To investigate the effect of coupling on spring behavior, two other similar springs without coupling between spring circular arcs are used for comparison, as shown in Fig. 2. Fig. 2a is a spring similar to Fig. 1; however, the connections between the spring circular arcs are removed. This spring is called the Type B. Fig. 2b is a different spring type similar to Fig. 2a, the serpentine springs in this case are not axial symmetry such as Type B, which has rotational symmetry, this spring is called the Type C. The two springs, Type B and Type C, are similar to that reported previously [12–14]. Therefore, the advantage of the coupling effect in the proposed spring is also preserved in comparison with springs without coupling.

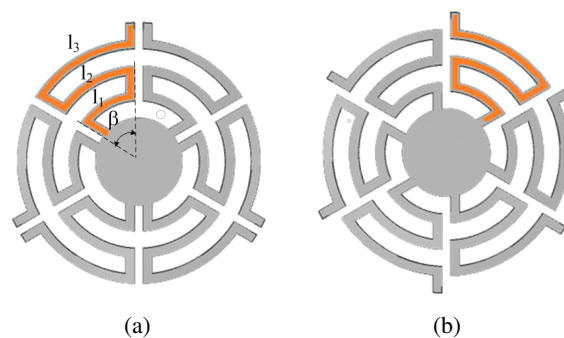


Fig. 2. System of axial symmetry spring (a) and rotational symmetry (b) using six serpentine springs composed of circular spring arcs

Furthermore, the operational frequency range is different for each application [3, 15, 16]. The operational frequency of MEMS devices depends on the dimensional parameters of spring. We can change the dimensional parameters of spring

as well as extending the length of spring by adding more spring stages, but the effect of the spring couplings in suppressing mode coupling is still preserved when compared with the similar spring systems without coupling. Therefore, in this study, we choose the spring system with three stages, as shown in Figs 1 and 2.

3. Models for calculating the stiffness of spring systems

3.1. Approximate method of straight beams connected in series

Equivalent model of the coupling spring consisting of components connected in series and parallel is shown in Fig. 3. The stiffness of the coupling spring is determined by:

$$K_t = 6K_b. \quad (1)$$

Here, K_b is the stiffness of a single serpentine spring as shown in orange color in Fig. 3. The number “6” represents the coupling spring consisting of six serpentine springs connected in parallel. In the current design, each serpentine spring consists of three circular arcs. So, the stiffness K_b is determined by:

$$\frac{1}{K_b} = \sum_{i=1}^n \frac{1}{k_i}. \quad (2)$$

k_i is the stiffness of the i -th circular arc spring, n represents the serpentine spring with n circular arcs. Approximately, the i -th circular arc can be considered as a straight beam of effective length l_i . The stiffness of the i -th straight beam spring is [26]:

$$k_i = \frac{3EI}{l_i^3}. \quad (3)$$

In Eq. (3), $I (= wt^3/3)$ is the moment of inertia of the straight beam spring, E is the Young’s modulus of the spring material, for the silicon material $E = 1.69 \cdot 10^{11}$ N/m.

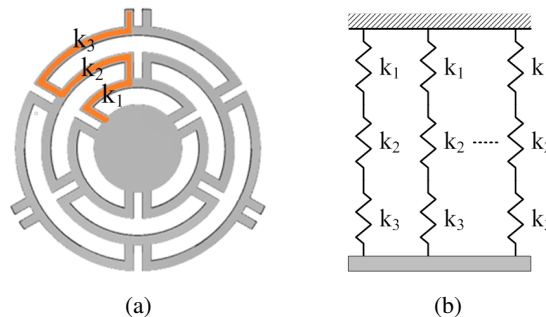


Fig. 3. Structure model of the coupling spring analyzed into equivalent mechanical structure model for evaluating stiffness (a) and equivalent spring model consisting of spring components connected in series (b)

The natural frequency of the coupling spring is determined by:

$$f = \frac{1}{2\pi} \sqrt{\frac{K_t}{m}}. \quad (4)$$

Here, m is the mass of the suspension consisting of the central plate and the serpentine spring beams. m is calculated by the formula:

$$m = m_{\text{plate}} + \frac{13}{35} m_{\text{beam}}, \quad (5)$$

where, m_{plate} is the mass of the central plate and m_{beam} is the total mass of the beams:

$$m_{\text{plate}} = \rho V_{\text{plate}} = \rho \pi R^2 t,$$

$$m_{\text{beam}} = 6\rho \sum_{i=1}^6 V_{\text{beam}_i} = \rho \pi R^2 t,$$

in which $V_{\text{beam}_i} = l_i w t$, w and t are constant for each design, however, l_i , the length of the i -th beam, is changed, and ρ is the density of spring material. The length of the i -th circular arc spring is determined by:

$$l_i = r_i \beta. \quad (6)$$

Here, $r_i = R + i(L_{IB} + w)$ is the radius of the i -th spring arc and $\beta = 60^\circ$ in this study.

3.2. Equivalent Sigitta spring system method

In this method, the equivalent spring model is shown in Fig. 4. Fig. 4a illustrates mechanical structure divided into the unit Sigitta springs, Fig. 4b illustrates three equivalent unit springs connected in series and Fig. 4c illustrates a Sigitta-shaped

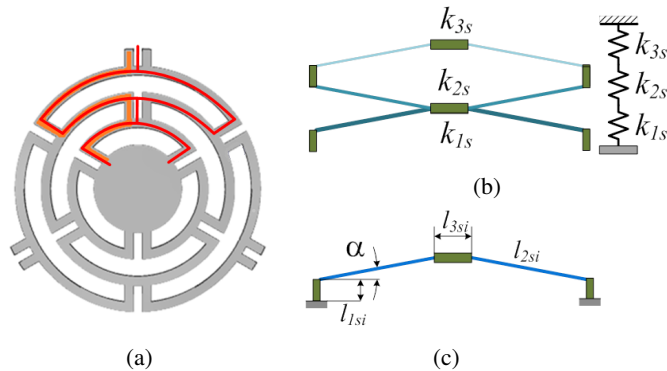


Fig. 4. Equivalent Sigitta spring system of the coupled spring

spring structure with the structural parameters used for the stiffness calculation. For the mechanical structure in the present study, the total spring consists of three component springs in Fig. 4b connected in parallel. Therefore, the total spring stiffness (K_{TS}) is:

$$K_{TS} = 3K_{3SSS}, \quad (7)$$

where, K_{3SSS} is the total stiffness of the spring in Fig. 4b, K_{3SSS} is determined by:

$$\frac{1}{K_{3SSS}} = \frac{1}{k_{1s}} + \frac{1}{k_{2s}} + \frac{1}{k_{3s}}. \quad (8)$$

The stiffness of a i -th Sigitta spring (k_{IS} with $i = 1, 2$, and 3) is calculated by [26]:

$$\begin{aligned} k_{IS} = 12 \left\{ 6 \left[(l_{3si} - 2c_i)^2 \sin^2 \alpha + 2(l_{1si} + 2l_{2si} \sin \alpha) \left[l_{1si} \cos \alpha \right. \right. \right. \\ \left. \left. \left. + (2l_{2si} \cos \alpha + l_{3si} - 2c_i) \sin \alpha \right] \cos \alpha \right] / (GI_t) + \left[6l_{1si}^2 + 14l_{2si}^2 \right. \right. \\ \left. \left. + 3(l_{3si} - 2c_i)^2 + 3 \left[(l_{3si} - 2c_i)^2 - 2(l_{1si}^2 + l_{2si}^2) \right] \cos 2\alpha \right. \right. \\ \left. \left. - 6(2c_i - l_{3si})(l_{2s} - 2l_{1si} \sin \alpha) \cos \alpha + 6l_{2si} \left[(l_{3si} - 2c_i) \cos 3\alpha \right. \right. \right. \\ \left. \left. \left. + l_{2si} \cos 4\alpha + 4l_{1si} \sin \alpha - 2l_{1si} \sin 3\alpha \right] \right] / (EI_y) \right\}^{-1} / l_{2si}, \quad (9) \end{aligned}$$

where, $G (= E/2(1+\nu))$, ν is the Poisson's ratio) is the shear modulus, $l_{1si} (= L_{IB})$ is the length of the connecting beam, l_{2si} is the length of the i -th circular arc spring and the length l_{3si} (Fig. 4c) is

$$l_{3si} = w + L_{IS}. \quad (10)$$

Here, $I_y (= wt^3/12)$ and $I_t (= wt^3/3)$ are the moment of inertia about the y and z axes, respectively. In this study, $\alpha = 30^\circ$. The parameter c_i in Eq. (9) is calculated by:

$$\begin{aligned} c_i = \left\{ GI_t \left[l_{3si} \cos \alpha + l_{2si} \cos 2\alpha \right] \cos \alpha + (EI_y - GI_t) l_{1si} \sin \alpha \cos \alpha \right. \\ \left. + EI_y (l_{3si} + 2l_{2si} \cos \alpha) \sin^2 \alpha \right\} / \left[2 \left(GI_t \cos^2 \alpha + EI_y \sin^2 \alpha \right) \right]. \quad (11) \end{aligned}$$

3.3. Equivalent serpentine spring system

In this method, the overall spring is considered to be composed of six identical serpentine springs, coupled in parallel, each serpentine spring shown in Fig. 2. The total spring stiffness in this model is calculated by $K_{TS} = 6K_{zS}$. The stiffness of each serpentine spring component K_{zS} is determined by [27]:

$$K_{zS} = 1 / \left[\sum_{n=1}^3 60n \sqrt{\frac{nw\sqrt{L_{IB}}}{l_n t}} \frac{l_n^2}{Gh} \left[\left(\frac{Gh}{EI_y} \right) l_n + 3L_{IB} \right] \right], \quad (12)$$

where, the parameter h is determined by [28]:

$$h = tw^3 \left[\frac{1}{3} - 0.21 \frac{w}{t} \left(1 - \frac{w^4}{12t^4} \right) \right]. \quad (13)$$

l_i in Eq. (12) is the length of the i -th arcs as shown in Fig. 2.

4. Comparing the performance of the spring types based on simulation

First, the simulation results of operating modes of spring systems are presented. Based on simulation, we will evaluate the mechanical coupling between the operation modes, the out-of-plane z -axis oscillation mode and nearest oscillation mode. Figs 5a–c show the first modes of the springs, which are also the modes oscillating in the z -axis direction, and Figs 5d–f show the second modes of oscillation. The parameters of the spring used in the simulation are $R = 50 \mu\text{m}$, $w = 20 \mu\text{m}$, $t = 10 \mu\text{m}$, $L_{IS} = 10 \mu\text{m}$ and $L_{IB} = 20 \mu\text{m}$. To consider the effect of the mechanical coupling on the spring system, we consider the frequency difference (δ_f) between the operating mode, mode z ($f_{\text{Mode } z}$) and the second mode ($f_{\text{Mode } 2}$)

$$\delta_f = (f_{\text{Mode } 2} - f_{\text{Mode } z}) / f_{\text{Mode } z} \times 100\%. \quad (14)$$

$f_{\text{Mode } z}$ and $f_{\text{Mode } 2}$ in this case are also shown in Figs 5a–c and Figs 5d–f, respectively. Therefore, the δ_f values for the three types of springs, type A ($\delta_{f\text{-type A}}$),

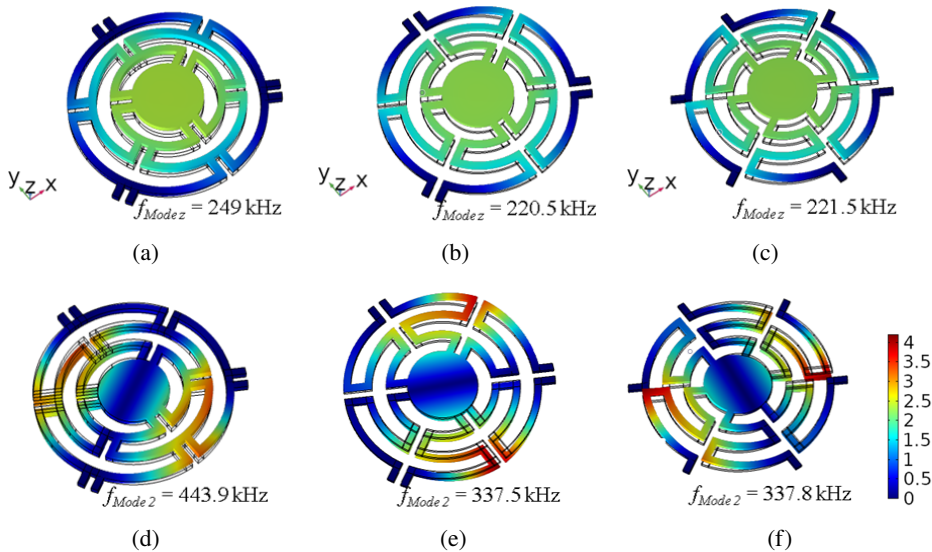


Fig. 5. Out-of-plane z -axis oscillation mode (a)–(c) and the second modes (d)–(f).

In this case, the spring system parameters are as follows $R = 50 \mu\text{m}$, $w = 20 \mu\text{m}$, $t = 10 \mu\text{m}$, $L_{IS} = 10 \mu\text{m}$ and $L_{IB} = 20 \mu\text{m}$

type B ($\delta_{f\text{-type B}}$), and type C ($\delta_{f\text{-type C}}$) are 60.8%, 52.8%, and 53.1%, respectively. Thus, according to the analysis of the coupling between operating modes, the system ensures mechanical isolation between the operating mode and neighboring modes [29].

To compare the performance of three spring types, we will investigate the effect of the mode coupling based on evaluating the dependence of δ_f on the representative dimensions of the spring. First, the width w of spring is changed from 2 μm to 20 μm , while the other parameters are kept constant, as shown in Fig. 5. The investigated results are shown in Fig. 6, where Figs 6a–d are frequencies of mode z and mode 2, the stiffness of mode z , and δ_f of three spring types, respectively.

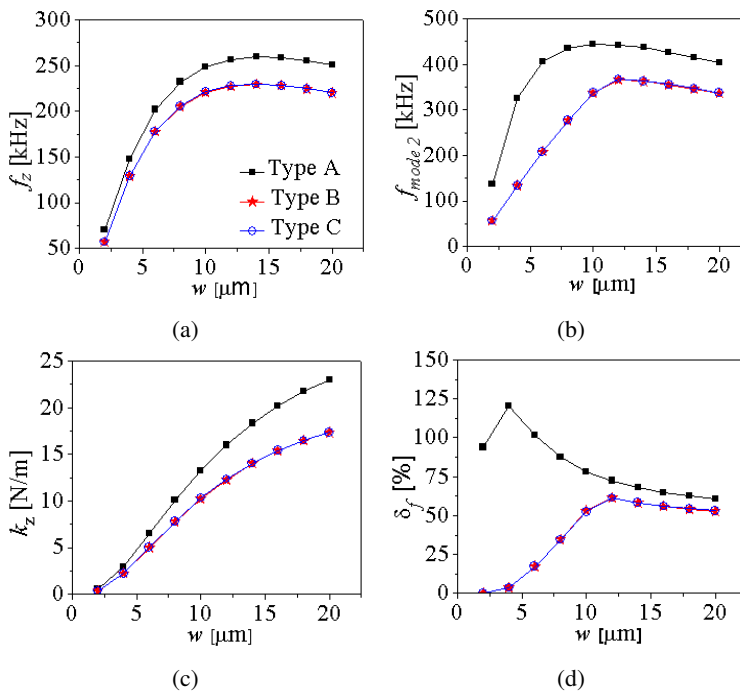


Fig. 6. Frequency of mode z (a) and mode 2 (b), the stiffness of mode z (c) and δ_f (d) of the three types of spring investigated as a function of w

Thus, the operating frequency of the three types of spring can be changed from 70 kHz to 260 kHz for Type A and from 55 kHz to 220 kHz for types B and C. The frequency characteristic of mode z and mode 2 initially increases and reaches a maximum then decreases gradually as the width of the circular arc spring increases. The investigation results also show that Type B and Type C have the same frequency value and δ_f . Especially, when the width w of circular arc spring increases, δ_f of the spring Type A is almost decreased, but is always greater than 60% and the value δ_f of the two remaining spring types.

In the next investigation, we change t from 2 μm to 20 μm while keeping other parameters as shown in Fig. 5. The investigated results are shown in Fig. 7. Thus, the oscillation frequency of mode z of all the three spring types is proportional to the thickness t of the circular arc spring. The operating frequency range of Type A varies from 50 kHz to 375 kHz, while types B and C vary from 50 kHz to 310 kHz. The operating frequencies of mode z and mode 2 as well as δ_f of the two spring types B and C in this investigation have the same values. The δ_f value of type A increases quite linearly from 75% to 90% as t increases gradually from 2 μm to 20 μm . In contrast, δ_f of types B and C tends to decrease from about 65% to 5% within the investigated t range.

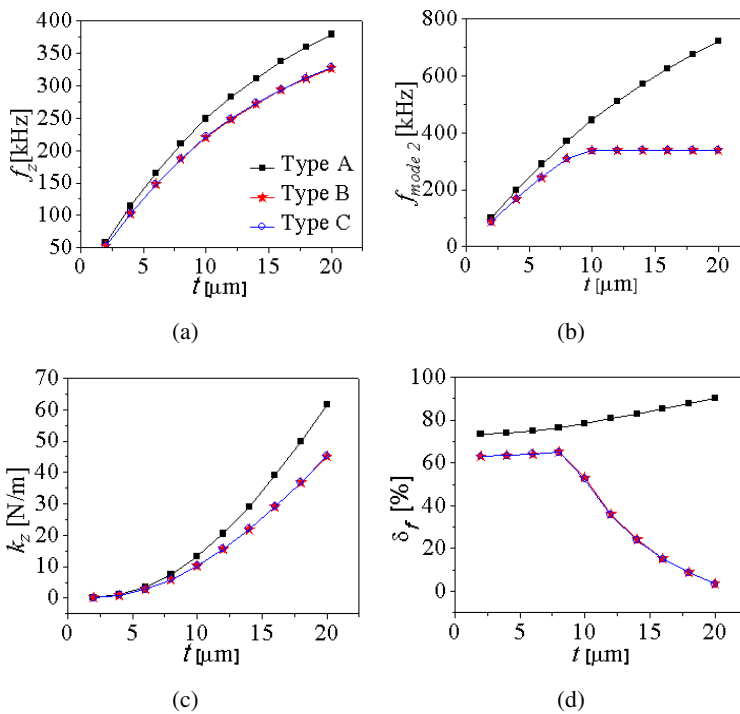


Fig. 7. Frequency of mode z (a) and mode 2 (b), the stiffness of mode z (c) and δ_f (d) of the three spring types investigated as a function of t

In the next study, we will investigate the behavior of three spring types depending on L_{IB} . Similarly, we also fix the remaining parameters of the spring systems, while changing the L_{IB} from 2 μm to 20 μm . The simulation results are shown in Fig. 8. When the L_{IB} increases, the length l_i of the spring circular arc increases, the investigation results in Fig. 8 show that the oscillation frequency of all three spring types tends to decrease. The frequency change range of mode z of Type A is about 600 kHz, while that of types B and C are about 550 kHz. The operation frequency of the springs Type B and Type C is still the same, but their second oscillation

mode has a separation as shown in Fig. 8b. The spring Type A has $\delta_f > 60\%$ and gradually increases to 78% when L_{IB} increases from 2 μm to 20 μm . In contrast, the δ_f value of types B and C tends to decrease as the L_{IB} increases and is always smaller than that of Type A.

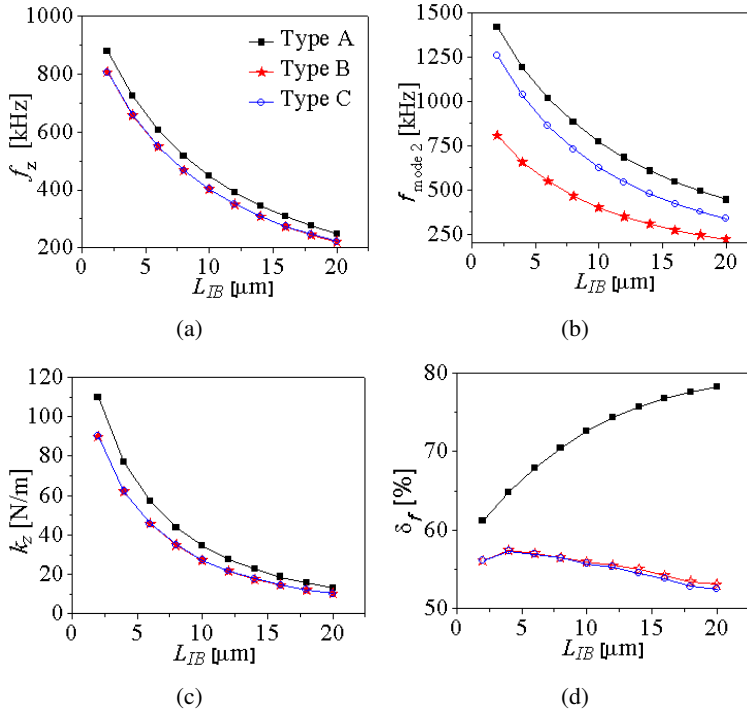


Fig. 8. Frequency of mode z (a) and mode 2 (b), the stiffness of mode z (c) and δ_f (d) of the three types of spring investigated as a function of L_{IB}

In the final case, we investigate the performance of three spring types depending on L_{IS} from 2 μm to 20 μm . The simulation results are shown in Fig. 9. The investigation results show that the operation frequencies of all three spring types tend to increase quite linearly, but with a reasonable frequency change range of about 50 kHz. The operation frequency of types B and C is also the same. The spring Type A has $\delta_f > 75\%$ and increases gradually to 85% when the L_{IS} increases from 2 μm to 20 μm . In contrast, the δ_f value of types B and C tends to decrease as the L_{IS} increases.

Thus, the investigation results in Figs 6 to 9 show that the spring Type A always has δ_f superior to the two remaining spring types. The behavior of springs Type B and Type C is not changed when the arrangement of springs in axial or rotating symmetry. Therefore, using the coupling bars among single serpentine springs in the plane, the spring type A has increased resistance to mode coupling, while the operating frequency range is similar to that of Type B and Type C.

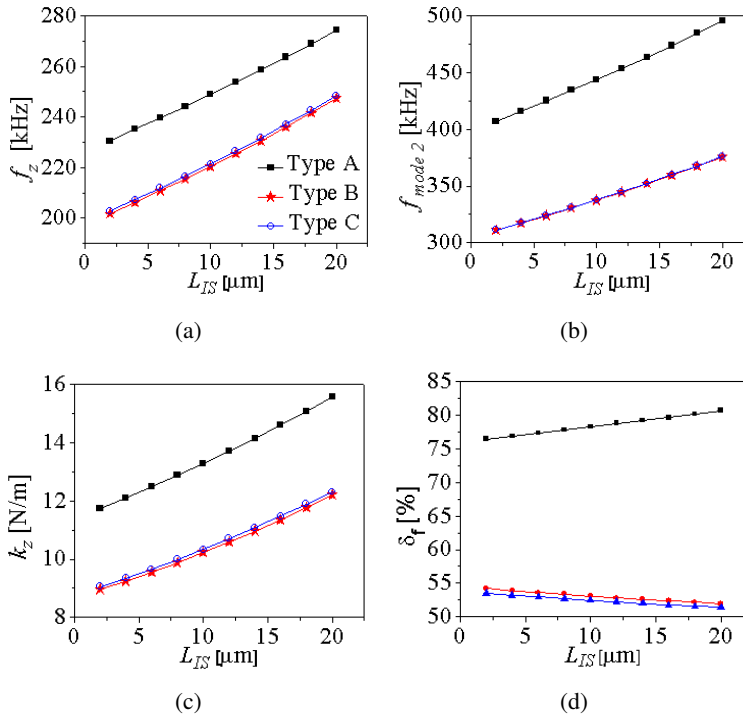


Fig. 9. Frequency of mode z (a) and mode 2 (b), the stiffness of mode z (c) and δ_f (d) of the three types of spring investigated as a function of L_{IS}

5. Comparing between the analytical and numerical solutions

In the above section, the operational simulation results of the three spring types have been presented, the spring Type A shows the superior characteristics compared to types B and C, while the performance characteristics of Type B are similar to that of Type C. Therefore, in this section we will focus on examining the computational models that can be applied for the design of micro-actuators based on the springs Type A and Type B as well as Type C. For convenience in comparison, we use the following symbols: Δf 1-A, Δf 2-A, and Δf 3-A are the difference between the calculated natural frequency (f_c) and the natural frequency obtained by using FEM (f_m) using the calculation methods 1, 2, and 3 for Type A, respectively; while Δf 1-B and Δf 3-B are the difference between f_c and f_m using the calculation methods 1 and 3 for Type B, respectively. Here, the difference between f_c and f_m is evaluated in percent by Δf i-A(B) = $(f_c - f_m) / f_m \times 100\%$. In the following, we consider the cases of the dimensional parameter change of the springs similar to that investigated by using FEM above. The calculated results using the three models in Section 2 are compared to numerical solutions using FEM. The Δf errors between the analytical and numerical solutions are shown in

Fig. 10. Fig. 10a shows that the error in the range of beam width from 2–6 μm is larger than 20%; however, in the range from 8–20 μm , the error is less than 10%. When the beam width changes, the Sigitta model is consistent with the structure of the coupled spring, while the straight beam spring model is suitable for the structure of the uncoupled springs.

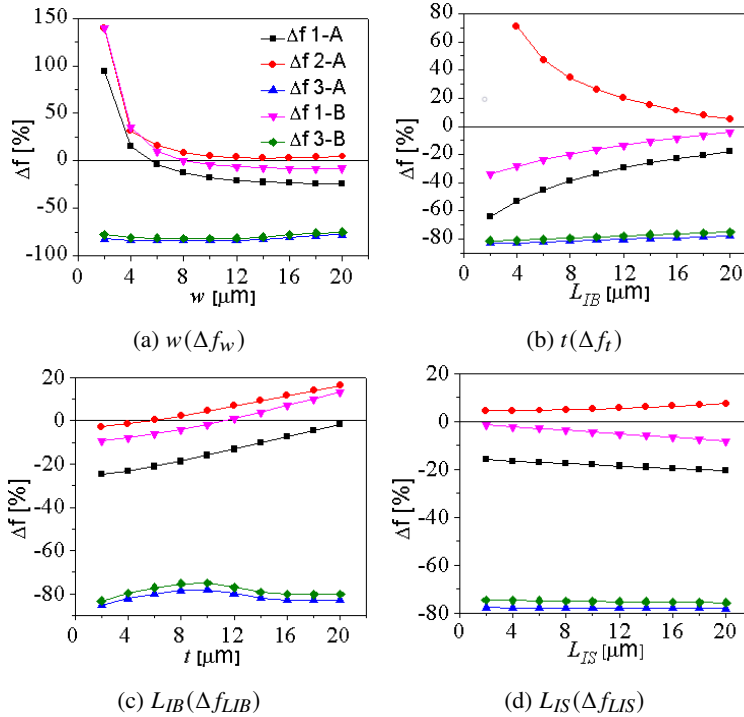


Fig. 10. Comparing the results of natural frequency calculation using the theoretical models in Section 2 and the numerical solutions in Section 3 depending on the representative dimensions of the springs

When the beam thickness changes, Fig. 10b, the calculation error using the Sigitta model for the coupled spring structure and that using the straight beam spring model for the uncoupled spring are less than 15%. The difference between the straight beam spring model and the coupled spring structure is from 5 to 25%. When the interconnection length L_{IB} between the beams changes from 2 to 10 μm , Fig. 10c, the Δf values are larger than 20%. However, when this length increases from 14 to 20 μm , Δf decreases and less than 10%. Finally, the Δf errors when the coupling length L_{IS} changes is shown in Fig. 10d. When changing the coupling length between two springs, the difference between the Sigitta model for the coupled spring structure and the straight beam spring model for the uncoupled spring structure is less than 10%. Meanwhile, the Δf values using the straight beam spring model for the uncoupled and coupled spring structures are larger than 15%.

From the above comparison, it shows that the Siggitta spring model is suitable for the structure of the coupled spring, while the straight beam spring model is suitable for the uncoupled spring structures. These models show small calculation errors ($< 10\%$) when the beam width is from 8 to 20 μm , the beam thickness from 2 to 20 μm , the interconnection length between circular spring arcs from 12 to 20 μm , and the coupling length between two serpentine springs from 2 to 20 μm . This suitability can be explained that the straight beam spring model does not take into account the coupling between the serpentine springs, while the equivalent Siggitta model has considered this coupling effect. In addition, the Siggitta model has also taken into account the angular deflection α of the spring beams (Fig. 4c), which is more suitable for the simulated spring structures than the approximated straight beam spring structure.

6. Conclusions

Thus, we have proposed a model of coupled spring that prioritizes to the out-of-plane oscillation while suppressing neighboring modes of oscillation. Compared with similar springs without coupling between component spring beams in plane, the coupling spring has shown outstanding characteristic in resistance to mode coupling. The difference between the operational frequency and adjacent modes is always greater than 60%, while the operational frequency can be varied in a wide range from 70 kHz to 900 kHz. In addition, in this study, the models for calculating the natural frequency of spring models have also been built. Comparing between the analytical and numerical solutions shows that the Siggitta spring model is suitable for the coupled spring structure, while the straight beam spring model is suitable for the uncoupled spring structures.

Acknowledgements

This research is funded by the Hanoi University of Science and Technology (HUST) under project number T2020-SAHEP-024, Vietnam.

References

- [1] X. Liu, K. Kim, and Y. Sun. A MEMS stage for 3-axis nan positioning. *Journal of Micromechanics and Microengineering*, 17(9):1796–1802, 2007. doi: [10.1088/0960-1317/17/9/007](https://doi.org/10.1088/0960-1317/17/9/007).
- [2] R. Legtenberg, A.W. Groeneveld, and M. Elwenspoek. Comb-drive actuators for large displacements. *Journal of Micromechanics and Microengineering*, 6(3):320–329, 1996. doi: [10.1088/0960-1317/6/3/004](https://doi.org/10.1088/0960-1317/6/3/004).
- [3] S. Abe, M.H. Chu, T. Sasaki, and K. Hane. Time response of a microelectromechanical silicon photonic waveguide coupler switch. *IEEE Photonics Technology Letters*, 26(15):1553–1556, 2014. doi: [10.1109/lpt.2014.2329033](https://doi.org/10.1109/lpt.2014.2329033).

- [4] T.Q. Trinh, L.Q. Nguyen, D.V. Dao, H.M. Chu, and H.N. Vu, Design and analysis of a z-axis tuning fork gyroscope with guided-mechanical coupling. *Microsystem Technologies*, 20(2):281–289, 2014. doi: [10.1007/s00542-013-1947-0](https://doi.org/10.1007/s00542-013-1947-0).
- [5] Y.J. Huang, T.L. Chang, and H.P. Chou. Novel concept design for complementary metal oxide semiconductor capacitive z-direction accelerometer. *Japanese Journal of Applied Physics*, 48(7):076508, 2009. doi: [10.1143/jjap.48.076508](https://doi.org/10.1143/jjap.48.076508).
- [6] A. Sharaf and S. Sedky. Design and simulation of a high-performance Z-axis SOI-MEMS accelerometer. *Microsystem Technologies*, 19(8):1153–1163, 2013. doi: [10.1007/s00542-012-1714-7](https://doi.org/10.1007/s00542-012-1714-7).
- [7] Y. Matsumoto, M. Nishimura, M. Matsuura, and M. Ishida. Three-axis SOI capacitive accelerometer with PLL C–V converter. *Sensors and Actuators A: Physical*, 75(1):77–85, 1999. doi: [10.1016/s0924-4247\(98\)00295-7](https://doi.org/10.1016/s0924-4247(98)00295-7).
- [8] D. Peroulis, S.P. Pacheco, K. Sarabandi, and L.P.B. Katehi. Electromechanical considerations in developing low-voltage RF MEMS switches. *IEEE Transactions on Microwave Theory and Techniques*, 51:259–270, 2003. doi: [10.1109/TMTT.2002.806514](https://doi.org/10.1109/TMTT.2002.806514).
- [9] Y. Liu. Stiffness Calculation of the microstructure with crab-leg flexural suspension. *Advanced Materials Research*, 317-319:1123–1126, 2011. doi: [10.4028/www.scientific.net/AMR.317-319.1123](https://doi.org/10.4028/www.scientific.net/AMR.317-319.1123).
- [10] H.M. Chou, M.J. Lin, and R. Chen. Investigation of mechanics properties of an awl-shaped serpentine microspring for in-plane displacement with low spring constant-to-layout area. *Journal of Micro/Nanolithography MEMS and MOEMS*, 15(3):035003, 2016. doi: [10.1117/1.JMM.15.3.035003](https://doi.org/10.1117/1.JMM.15.3.035003).
- [11] D.V. Hieu, L.V. Tam, N.V. Duong, N.D. Vy, and C.M. Hoang. Design and simulation analysis of a z axis microactuator with low mode cross-talk. *Journal of Mechanics*, 36(6):881–888, 2020. doi: [10.1017/jmech.2020.48](https://doi.org/10.1017/jmech.2020.48).
- [12] D.V. Hieu, L.V. Tam, K. Hane, and M.H. Chu. Design and simulation analysis of an integrated XYZ micro-stage for controlling displacement of scanning probe. *Journal of Theoretical and Applied Mechanics*, 59(1):143–156, 2021. doi: [10.15632/jtam-pl/130549](https://doi.org/10.15632/jtam-pl/130549).
- [13] F. Hu, W. Wang, and J. Yao. An electrostatic MEMS spring actuator with large stroke and out-of-plane actuation. *Micromechanics and Microengineering*, 21(11):115029, 2011. doi: [10.1088/0960-1317/21/11/115029](https://doi.org/10.1088/0960-1317/21/11/115029).
- [14] W. Wai-Chi, A.A. Azid, and B.Y. Majlis. Formulation of stiffness constant and effective mass for a folded beam. *Archives of Mechanics*, 62(5):405–418, 2010.
- [15] Y. Cao and Z. Xi. A review of MEMS inertial switches. *Microsystem Technologies*, 25(12):4405–4425, 2019. doi: [10.1007/s00542-019-04393-4](https://doi.org/10.1007/s00542-019-04393-4).
- [16] K.R. Sudha, K. Uttara, P.C. Roshan, and G.K. Vikas. Design and analysis of serpentine based MEMS accelerometer. *AIP Conference Proceedings*, 1966:020026, 2018. doi: [10.1063/1.5038705](https://doi.org/10.1063/1.5038705).
- [17] H.M. Chou, M.J. Lin, and R. Chen. Fabrication and analysis of awlshaped serpentine microsprings for large out-of-plane displacement. *Journal of Micromechanics and Microengineering*, 25:095018, 2015. doi: [10.1088/0960-1317/25/9/095018](https://doi.org/10.1088/0960-1317/25/9/095018).
- [18] C.M. Hoang, and K. Hane. Design fabrication and vacuum operation characteristics of two-dimensional comb-drive micro-scanner. *Sensors and Actuators A: Physical*, 165(2): 422–430, 2011. doi: [10.1016/j.sna.2010.11.004](https://doi.org/10.1016/j.sna.2010.11.004).
- [19] G. Barillaro, A. Molfese, A. Nannini, and F. Pieri. Analysis simulation and relative performances of two kinds of serpentine springs. *Journal of Micromechanics and Microengineering*, 15(4):736–746, 2005. doi: [10.1088/0960-1317/15/4/010](https://doi.org/10.1088/0960-1317/15/4/010).

- [20] P.B. Chu, I. Brener, C. Pu, S.S. Lee, J.I. Dadap, S. Park, K. Bergman et al. Design and nonlinear servo control of MEMS mirrors and their performance in a large port-count optical switch. *Journal of Microelectromechanical Systems*, 14(2):261–273, 2005. doi: [10.1109/JMEMS.2004.839827](https://doi.org/10.1109/JMEMS.2004.839827).
- [21] G.D.J. Su, S.H. Hung, D. Jia, and F. Jiang. Serpentine Spring corner designs for micro-electro-mechanical systems optical switches with large mirror mass. *Optical Review*, 12(4):339–344, 2005. doi: [10.1007/s10043-005-0339-9](https://doi.org/10.1007/s10043-005-0339-9).
- [22] A. Khelif, A. Ahmed, S. Pandit, B. Mezghani, R. Patkar, P. Dixit, and M.S. Baghini. Experimental and theoretical dynamic investigation of MEMS Polymer mass-spring systems. *IEEE Sensors Journal*, 20(19):11191–11203, 2020. doi: [10.1109/JSEN.2020.2996802](https://doi.org/10.1109/JSEN.2020.2996802).
- [23] J. Wu, T. Liu, K. Wang, and K. Sørby. A measuring method for micro force based on MEMS planar torsional spring. *Measurement Science and Technology*, 32(3):035002, 2020. doi: [10.1088/1361-6501/ab9acd](https://doi.org/10.1088/1361-6501/ab9acd).
- [24] Z. Rahimi, J. Yazdani, H. Hatami, W. Sumelka, D. Baleanu, and S. Najafi. Determination of hazardous metal ions in the water with resonant MEMS biosensor frequency shift – concept and preliminary theoretical analysis. *Bulletin of the Polish Academy of Sciences: Technical Sciences*, 68(3): 529–537, 2020. doi: [10.24425/bpasts.2020.133381](https://doi.org/10.24425/bpasts.2020.133381).
- [25] K.G. Sravani, D. Prathyusha, C. Gopichand, S.M. Maturi, A. Elsinawi, K. Guha, and K.S. Rao. Design, simulation and analysis of RF MEMS capacitive shunt switches with high isolation and low pull-in-voltage. *Microsystem Technologies*, 28:913–928, 2022. doi: [10.1007/s00542-020-05021-2](https://doi.org/10.1007/s00542-020-05021-2).
- [26] N. Lobontiu and E. Garcia. *Mechanics of Microelectromechanical Systems*. Kluwer Academic Publishers, 2005. doi: [10.1007/b100026](https://doi.org/10.1007/b100026).
- [27] H.A. Rouabah, C.O. Gollasch, and M. Kraft. Design optimisation of an electrostatic MEMS actuator with low spring constant for an “Atom Chip”. In *Technical Proceedings of the 2005 NSTI Nanotechnology Conference and Trade Show*, volume 3, pages 489–492, 2002.
- [28] R. Raymond and J. Raymond. *Roark’s Formulas for Stress and Strain*. McGraw-Hill, 1989.
- [29] M.S. Weinberg and A. Kourepenis. Error sources in in-plane silicon tuning-fork MEMS gyroscopes. *Journal of Microelectromechanical Systems*, 15(3):479–491, 2006. doi: [10.1109/jmems.2006.876779](https://doi.org/10.1109/jmems.2006.876779).